Received September 28, 2015, accepted October 14, 2015, date of publication October 30, 2015,
date of current version November 9, 2015.

Digital Object Identifier 10.1109/ACCESS.2015.2496122

Marine Vessel and Power Plant System Simulator

TORSTEIN I. BØ[1], ANDREAS R. DAHL[3], TOR A. JOHANSEN[1], EIRIK MATHIESEN[2], MICHEL R. MIYAZAKI[3], EILIF PEDERSEN[3], ROGER SKJETNE[3], ASGEIR J. SØRENSEN[3], LAXMINARAYAN THORAT[3], AND KEVIN K. YUM[3]

[1]Centre for Autonomous Marine Operations and Systems, Department of Engineering Cybernetics, Norwegian University of Science and Technology, Trondheim NO-7491, Norway
[2]Kongsberg Maritime AS, Kongsberg NO-3616, Norway
[3]Centre for Autonomous Marine Operations and Systems, Department of Marine Technology, Norwegian University of Science and Technology, Trondheim NO-7491, Norway

Corresponding author: T. I. Bø (torstein.bo@ntnu.no)

This work was supported in part by the Research Council of Norway through the Project entitled Design to Verification of Control Systems for Safe and Energy Efficient Vessels with Hybrid Power Plants under Grant 223254/F50 and Grant 210670/070, in part by DNV GL, in part by the Kongsberg Maritime AS, and in part by the Research Council of Norway through the Centres of Excellence Funding Scheme–Centre for Autonomous Marine Operations and Systems, under Project 223254.

ABSTRACT Modern marine electric propulsion vessels have many systems. These interactions and integration aspects are essential when studying a system and subsystem behavior. This is especially important when considering fault scenarios, harsh weather, and complex marine operations. However, many simulators, including a selection presented here, study the positioning system and the power system separately. This paper proposes a simulator combining the two systems, as an extension to the marine systems simulator MATLAB/Simulink library. The intended use cases and the according design choices are presented. New subsystem models include a power-based electrical bus model and a simplified diesel engine model. Both are validated through the simulation against established models. In addition, established models for generators, electrical storage devices, thrusters, and a mean-value diesel engine model are summarized with rich references. Three case studies illustrate the multi-domain use of the simulator: 1) a semi-submersible drilling rig performing station keeping under environmental disturbances; 2) the same vessel subject to an electrical bus reconfiguration; and 3) a supply vessel with a hybrid power plant.

INDEX TERMS Marine technology, marine vehicles, power system simulation, dynamic positioning.

INTRODUCTION

A. SHIPBOARD ELECTRICAL SYSTEM

The onboard electric power system is crucial for most modern marine vessels conducting advanced operations. Diesel-electric propulsion is common in offshore oil and gas vessels and cruise/passenger ships with dynamic positioning (DP).

The ability to conduct stationkeeping and maneuvering subject to current, waves, and wind loads depends on the power plant capacity. Insufficient power may result in decreased DP performance and loss of position. More severely, a total loss of electric power, known as a blackout, results in loss of control of the vessel.

Redundancy in power capacity, distribution, and in the number of generating units is one possible alleviation of the risk of power system faults. However, redundancy is costly. Economical expenses are significant, both in terms of investment in equipment, which most of the time is not strictly necessary, and in terms of machine running hours leading to more frequent maintenance, and increased emissions and fuel consumption.

The mentioned concerns motive the development of new power plant control strategies and the introduction of new power sources. Such steps are not trivial, due to the complex and strongly interconnected nature of onboard marine power plants, and the weak grid, i.e., sensitive to changes both in produced and consumed power. Numerical simulation is a valuable tool for investigating such effects at all stages of design, implementation, and operation.

B. PREVIOUS WORK

A number of marine power plant simulation solutions exist. The intended use ranges from commercial to academic, and the content from a few state equations to complete software suites. A selection follows:

Marine Cybernetics' CyberSea technology platform encompasses models of hydrodynamics, electromechanics and sensors [1]. It is used for independent

hardware-in-the-loop (HIL) testing [2] and dynamic capability analysis (DynCap) [3].

U.S. Office of Naval Research's Electric Ship Research and Development Consortium studies include both HIL simulators [4], models of higher fidelity [5], and extension to hybrid plants [6].

Marine Systems Simulator (MSS) [7] library and simulator for MATLAB/Simulink is a 2004 merge of [8, Sec. 1]: marine GNC toolbox [9], MCSim [10], and DCMV [11]. It has vessel dynamics, environmental (wave, surface current, and wind) loads and advanced thruster models.

DNV GL's Sesame Marine [12] risk management software includes Marintek's SImulation of Marine Operations (SIMO) motion and stationkeeping simulator. The system is capable of modeling multibody systems and flexible systems.

Italian Integrated Power Plant Ship Simulator includes an integrated power system model implemented in the Simulink environment [13].

NTNU models include thruster power consumption [14] and power management system functions [15].

NTNU bond graph model library [16] includes a vessel model. The library is also verified through full-scale experiments.

Some solutions mainly focus on the electrical system without concern for the actual DP performance and related consumption, while others do the opposite.

C. DESIGN OF SYSTEM SIMULATORS

The simulator presented in this paper is a system simulator. This means that the purpose is to model interactions between each of the subsystems of the complete system, and it should be flexible, such that many different cases can be studied. A modular design achieves this.

The use cases of the simulator will determine the dynamics that we need to model and parameterize. The difference in magnitude of the smallest and the largest timescale of the dynamics in such a multi-physics simulator may be in order of decades. It is therefore essential to decide the important timescales for the particular study.

The smallest timescale of the vessel is, in the electric system, in the order of milliseconds. In the other end, quasistatic studies such as effects of wear and tear, are in the order of months and years. For simulating short-circuit, the fast dynamics must be modeled, while the effects of the environment, and wear and tear, can be assumed constant. On the other hand, the electric system can be assumed to be in steady state when simulating DP operation, as the timescales of the electric system are much smaller than the timescale of the vessel motion. Fig. 1 lists the time scale of the simulator components. For certain components model reductions should not take place, as discussed in respective sections later.

The complexity of a system simulator grows with the number of components and the fidelity level. By increasing

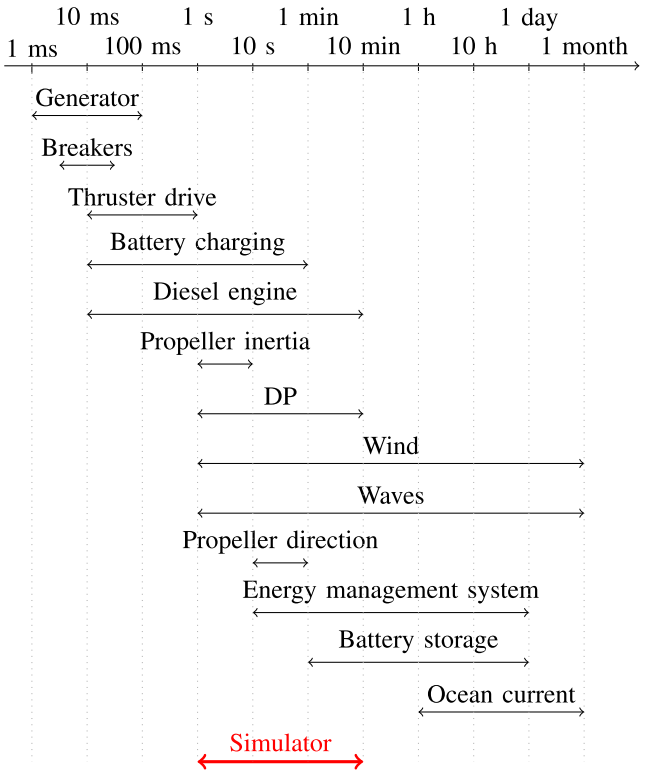

FIGURE 1. List of components in the simulator and their time scales.

the fidelity level, more parameters with higher order model structure, and a more thorough verification and validation are required. In addition the computational speed will typically be reduced. For studies where high fidelity level is required, not all the submodels need to be of high fidelity, as long as the model reduction is done properly and with care. By using a modular design, it is easy to use low fidelity models to identify where higher fidelity is required. These models can then be replaced with high fidelity models.

Verification and validation is challenging for system simulators due to the high complexity. Each submodel can be verified by itself, but this does not verify their integration. Small scale or full scale tests can be used for verification, but this is costly and time consuming. In many cases experiences from a set of trained operators are the most practical way of verifying expected system-level performance.

D. USE CASES

The simulator has been used in several studies considering DP with diesel-electric propulsion and consumers such as hotel loads and motors for drilling, compressors, and pumps.

A selection of typical use cases follows:

Realistic power consumption profile: Since the DP controller and thruster models are interconnected with the power plant, the power load fluctuations are represented in a realistic way. The interaction between the many control subsystems, such as PMS, thrust allocation, thruster torque or speed control, is included [17]. The simulator can therefore be used to generate time

series for later use in isolated subsystem simulation (e.g., diesel engine simulation).

Fault consequence analysis: The plant behavior in the event of an electrical fault, such as the loss of a genset, can be simulated [18]. The resulting DP performance is then also available. This may improve the conventional capability analysis, which is calculated assuming that the propulsion system is in steady-state. Indeed, transients during plant reconfiguration can be critical [3].

Operation optimization: The detailed level of modeling includes many states for each submodule, for instance temperature and power output. Based on these, operation may be optimized with regards to emissions, maintenance, or fuel consumption.

Concept evaluation: Submodules representing new subsystems such as energy storage device (ESD), can be interfaced to the simulator. This allows investigation of new power sources and their effect on the overall control and performance of the plant.

It must be stressed that the simulator is not limited to diesel-electric propulsion, nor DP operations.

E. CONTRIBUTION

This paper focuses on the models and methods needed for an integrated simulator of the electric power system together with the vessel motion including the DP system. Secondly, some new models are established and verified to achieve the desired fidelity level and performance. Most of the models are verified models from literature. The scope of the simulator runs from high-level control systems, such as the positioning system and power management system (PMS), to high-fidelity models of power generators, storage, and consumers, such as gensets, batteries, and thrusters, respectively. The accuracy of the simulator is only verified qualitatively due to the complexity of the system. Quantitative verification of the plant is research still to be done and is considered outside the scope of this article.

This paper is an extension of [19], including more details of the models. In addition, verification of the new models and new cases are presented.

F. OVERVIEW OF THE PAPER

This paper consists of three sections, the model is presented in Section I, the new models are verified in Section II, and simulations are shown in Section III. The modeling part starts with an overview of the simulator, followed by details of the power management system. The electrical components are then presented, with the switchboard and generator. Next, two models of diesel engines are presented, followed by the thruster models. Last is a presentation of the hydrodynamic model of the vessel, the environmental forces and the DP control system. In Part II, verification of the electric bus model and simplified diesel-engine model are presented. In the last part, a simulation of a drilling rig in DP operation, then simulation of a fault is shown, before a simulation with batteries is presented.

I. MODELING

A. SIMULATOR OVERVIEW

The main assumptions of the simulator are:

Steady-state electric system: It is assumed that the electrical system is in steady state, this is done to get real-time capabilities. The simulator captures dynamics with time scale down to 1 second. However, the dynamics of the electric system are often in milliseconds and are therefore assumed to be in steady state. This is verified in Section II-A. The simulated electrical variables are frequency, voltage, active power, and reactive power. It is therefore possible to simulate faults, such as under/over-frequency, slowly developing under/over voltage fault, and reverse power. However, it is not able to simulate phase imbalance, transient voltage faults, short-circuit, and harmonic distortion.

Mean-value engine model: The diesel engines are modeled by mean-value engine models. This means that most of the components in the diesel engine system are mathematically modeled based on the physical laws. However, the in-cylinder process is simplified so that it gives only a cycle average output such as average shaft torque, and mass and energy flow of the combustion gas.

Power management system: The objective of the PMS is to make sure that the power plant is safe and efficient. More details are given in Section I-B.

Protection relays: Protection relays are not modeled, as breakers can be tripped by a timer. This means that some custom protection relays need to be implemented to simulate a partial blackout. Alternatively, post-processing can be used to detect when breakers should be opened.

Fixed pitch, variable speed thrusters: The thrusters are assumed to be fixed pitch propellers, with the possibility to run with variable speed. Thrusters that can rotate in any direction, azimuth thrusters, and fixed direction thrusters (e.g., tunnel thrusters) can be simulated.

An object-oriented modeling structure has been used to model the marine power plant. This means that each block in the simulator represents a physical component in the vessel, and further subsystem blocks represent internal physical components of the larger system.

The top level view of the model is illustrated by an example in Fig. 2. This view represents the information flow for motion control of the vessel. A DP controller has been used in the presented case. Alternatively, the setpoints of the thrusters can be given manually during transit, maneuvering, or other operations without DP control.

For this case, the view contains:

1) Observer; estimates the position and velocity of the vessel from measurements.
2) DP control system; calculates a desired thrust command.

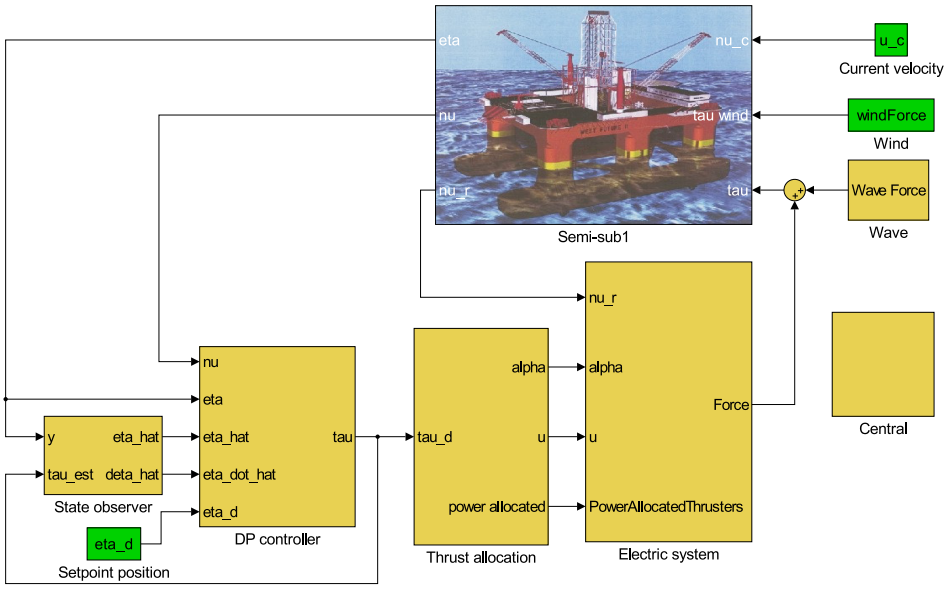

FIGURE 2. Example of top level view, including the vessel model, observer, DP controller, thrust allocation, and the electrical system. The electrical system is further presented in Fig. 3. The central block is used for common calculations.

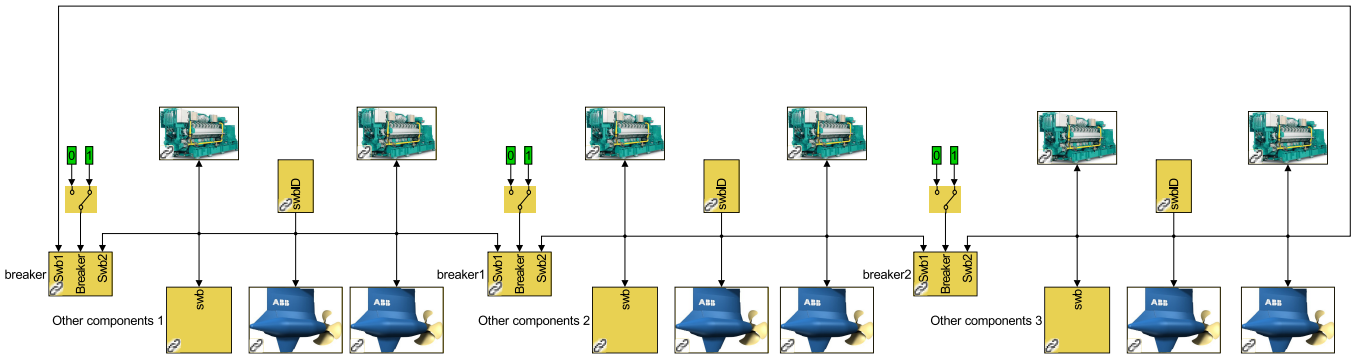

FIGURE 3. Example of power plant view, including the bus-tie breakers, thrusters, generator sets, and other loads block. This power plant is used for simulation of drilling rig in Section III.

3) Thrust allocation (TA); converts the desired thrust command for the vessel to thrust commands for each thruster.
4) Electric system with thruster model; converts the thrust command to actual thrust, and electric power consumption.
5) Environmental model; generates realistic loads for the environment.
6) Vessel model; calculates the motions of the vessel given the thruster and environmental loads.
7) Central; this block is used for common calculations.

The electric power plant is modeled inside the electric system block. An example of a power plant is shown in Fig. 3 and consists of:

1) Generator set; consisting of a prime mover (e.g., diesel engine), a generator, a speed governor, and an automatic voltage regulator (AVR).
2) Thruster drives; consisting of a frequency converter, an electric motor, a propeller, and controller.
3) Other components; this can be hotel and drilling loads, which are modeled as time series of power consumption. However, this block may also be used for energy storage, such as batteries with a frequency converter. The load is then negative when the block delivers power and positive when it consumes power.
4) Switchboards; connecting loads and producers.
5) Breakers; connecting and disconnecting components.

Simulink was chosen in order to extend the MSS toolbox [8] to include better thruster models and an electric power plant. The downside by choosing Simulink is the modeling of interconnections. The system is hard to divide into levels as required by the subsystem architecture of Simulink. We chose to use the top level model view for the vessel control. The electric power plant is a subsystem in this view and it is made to mimic a single line diagram. The stiff

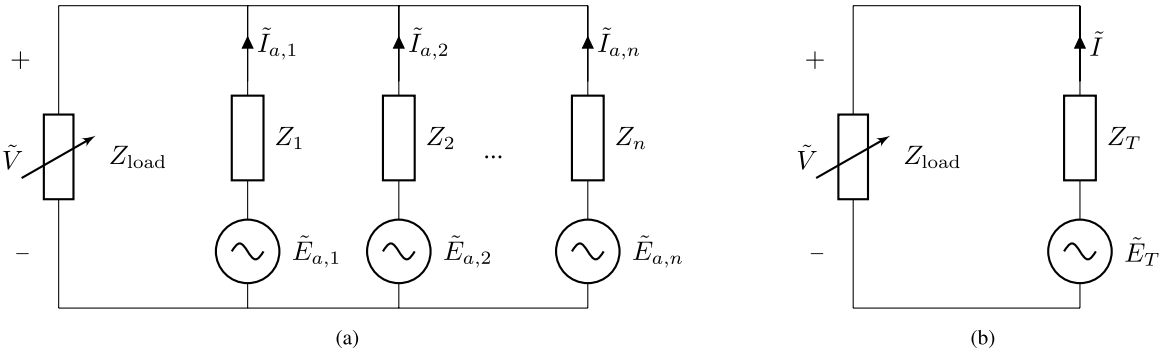

FIGURE 4. (a) Circuit diagram of bus with one load with the impedance Z_{load} and n generators. (b) Thevenin equivalent circuit of (a).

solver ode15s is used as numerical solver in the case study, since the local controllers give a stiff model.

Some first order lowpass filters are used to avoid algebraic loops, where the time constant of the filters are chosen to be smaller than the fastest dynamics of the relevant models. This is needed since we ignore some fast dynamics. The filters can therefore be seen as simplified models of the ignored dynamics. One example is the power available signal. An algebraic loop occurs since the power available is dependent on the power consumption, while the power available also constrains the power consumption. This is solved by adding a lowpass filter on the power available signal, which is faster than the time scale of the consumers. Alternatively, one may use discrete time and a delay for these signals, but this reduces the performance of the chosen implicit ode solver.

B. POWER MANAGEMENT SYSTEM

The objective of the PMS is to make sure there is always enough power available, to prevent blackout. If a blackout occurs, the power should be restored as fast as possible. The PMS starts additional generators when the excessive power capacity of the connected producers is too low. In addition, the PMS allocates power to the different consumers, by first summing the current power capacity of the producers, and then sharing this among the consumers based on their desired power consumption and priority. This signal, called *power available*, is sent to some consumers, stating the maximum power limit for the specific load. Load shedding (disconnection of consumers) is done in extreme cases, when power reduction must be done immediately (e.g., close to under-frequency).

Fast load reduction is an alternative method to reduce the power consumption quickly. It reduces the load of the thruster drives, since they can change the power consumption quickly due to the frequency converters. Shortly after the fault is cleared or the capacity is increased, the drives can increase their loads. This is in contrast to load shedding where the consumers often needs to be restarted after being disconnected.

The PMS can also adjust the droop and isochronous load sharing parameters to adjust the load sharing. This is done during progressive loading after connection of generator sets. Progressive loading is implemented to ensure that the power generation of the new producer is slowly increased from no load to desired load sharing.

The PMS algorithm is implemented in C++ as an S-function block and can easily be configured to different power plants. The object-oriented focus of the simulator is kept in the PMS implementation, so that new functionalities, such as automatic start and stop, can easily be added.

C. BUS VOLTAGE CALCULATION

The voltage of the bus is needed to calculate the load sharing of the generators. The generators are connected in parallel as shown in Fig. 4a. The loads are assumed to be independent of the bus voltage, their active and reactive power are therefore given. Thévenin equivalent circuit, as shown in Fig. 4b, of the connected generator sets is used to calculate the bus voltage. This circuit is closed by the loads, which have a known power consumption but unknown impedance.

This gives the equation

$$P_{\text{bus}} + jQ_{\text{bus}} = 3\tilde{V}\tilde{I}^* = 3\tilde{V}\frac{\tilde{E}_T^* - \tilde{V}^*}{Z_T^*}, \tag{1}$$

where P_{bus} and Q_{bus} are the active and reactive power of the loads, $\tilde{V}$ is the line-to-neutral bus voltage, $\tilde{I}$ is the current, $\tilde{E}_T$ is the Thévenin equivalent voltage, and Z_T is the Thévenin equivalent impedance. Equation (1) has either two solutions, one solution, or no solution. For the case where there exists two solutions, the solution with the largest absolute value for the bus voltage is used. The largest voltage yields a high resistance of the load, and a low current, hence low internal loss. The lower voltage solution gives a resistance smaller than the Thévenin equivalent resistance, which is unphysical. This yields a high current, with very high internal loss since most of the voltage drop occurs over the internal impedance.

During simulations it may occur that there exists no valid solution. This may happen when the load increases rapidly (a load is connected) or the Thévenin equivalent voltage of the generator decreases rapidly (fault in AVR or disconnection of a generator). In such cases, the voltage is set to a low value. This gives an incorrect load sharing, but the AVR will increase the voltage quickly. During the verification study

in Section II-A, a valid solution of the bus voltage was regained within 0.1 millisecond. This is permissible since the time is very short compared to the time scale of the mechanical system. A lowpass filter must therefore be added when simulating voltage protection relays.

D. GENERATOR

In marine power plants, synchronous generators are typically used to produce power. As mentioned earlier, the generator is assumed to be in steady state and with balanced phases. The electrical torque is

$$\tau_e = \frac{p + p_{\text{loss}}}{\omega} = \frac{p}{\omega} + \frac{r(p^2 + q^2)}{\omega v^2}, \tag{2}$$

where p and p_{loss} is the active power generated and power loss in the generator, r is the resistance in the stator windings, q is the reactive power, and v is the terminal voltage. The terminal line-to-neutral voltage is given as [20]:

$$\tilde{V}_a = -Z\tilde{I}_a + \tilde{E}_a, \tag{3}$$

where Z is the internal impedance of the generator set, $\tilde{I}_a$ is the current through phase a and $\tilde{E}_a$ is the induced line-to-neutral voltage for phase a.

It is assumed that the magnitude of $\tilde{E}_a$ is perfectly controlled by the AVR or at least the dynamics are much faster than the dynamics of the mechanical system. This is verified in Section II-A. The per phase angle of $\tilde{E}_a$ is

$$\angle\tilde{E}_a = \frac{\theta N_{\text{poles}}}{2}, \tag{4}$$

where θ is the mechanical angle and N_{poles} is the number of poles of the generator. Parameters are found from [20].

The AVR regulates the terminal voltage by manipulating the induced voltage. In this simulator, we use a droop controller to determine the setpoint, based on the reactive power of the generator set. This takes care of the reactive load sharing. The generators deliver equal amount of reactive power if they have equal voltage droop curves.

E. DIESEL ENGINE

The dynamics of the diesel engine are the slowest dynamics of a diesel-electric power plant. Most modern diesel engines are turbocharged to provide increased power density. When a turbocharged diesel engine needs to increase its delivered power, more air is required into the cylinders to avoid incomplete combustion and visible smoke in the exhaust. However, the response of the air system is slow, due to the rotating inertia of the turbocharger and the large air and exhaust receiver volumes. This gives rise to the *turbo-lag*. In addition, increasing the fuel injection rises the temperature in the cylinder.

Constraints are, therefore, added to the engine control output by the engine manufacturer to ensure that the fuel injection is not changed too quickly. This is done to avoid that the engine is damaged by a rapid change of temperature, and that the air pressure in the inlet manifold is large enough to allow for complete combustion. These constraints are in some cases conservative, and the air dynamics may be neglected since the engine will always run with complete combustion due to these constraints.

Transients of the diesel engines can be grouped into three categories [21]. The first is energy transfer delay which happens due to signal delay, preset valve closure or injection timing. The time scale of such phenomena is in milliseconds. In simulation, this can only be seen by detailed modeling of the cylinder process and the fuel injection system. Secondly, the already mentioned air dynamics are the most interesting physics in this kind of application. The typical transient time scale of the air dynamics is in seconds. Lastly, the thermal transients are caused by the thermal inertia of the system, which may have time scale of tens of minutes.

1) MEAN VALUE MODEL

The main purpose of the diesel engine simulation model is to capture the air dynamics including pressure before the engine cylinder which can be related to the charge air available for combustion. In the mean value engine model, most of the physics in the engine system components are captured except for the in-cylinder process, i.e., the thermodynamic cycle. The main components included in the model are an engine cylinder block, a turbocharger, a charge air cooler, an air receiver and an exhaust receiver. The implemented mean value engine model is based on the models presented in [22]–[27].

The engine system including a turbocharging system is inherently a thermodynamic process with gas mixture as medium. Therefore, main variables of the system are pressure, p; temperature, T; and fuel-air equivalent ratio, F. Also flow variables, such as mass flow of gas, $\dot{m}$; enthalpy flow or rate of change in internal energy, $\dot{E}$; and mass flow of burned fuel, $\dot{m}_{\text{b}}$, are necessary to describe the dynamics of the system.

A filling and emptying method [23] is used to construct the thermodynamic process model of the system. In this approach, the target model is constructed by placing control volumes in a series as configured in the real system and putting a flow restriction between adjacent control volumes. It is assumed that the thermodynamic states, such as pressure and temperature, are uniform within a control volume and that there is no accumulation of mass in the flow restriction. Then, all the components fall into two categories: a thermodynamic control volume or a flow restriction. Generally, pipes, receivers, and cylinders are thermodynamic control volumes; whereas any valve, port, compressor, turbine, and heat exchangers are considered as flow restrictions.

Thermal control volumes determine the thermodynamic states of the system. They consist of two parts. The first one is a flow junction where mass conservation and the first law of thermodynamics are implemented. The second part is the flow accumulation where the net rate of change in mass and energy are integrated. The integrated values are the mass, m_{cv}; the internal energy, U_{cv}; and the mass of burned fuel within the control volume, m_{f}; which are states of

the system. Pressure and temperature are derived from a table of thermodynamic properties, such as the JANAF table [28], and by using the equation of state (i.e. ideal gas law). In order to achieve faster simulations, a semi-empirical formula for thermodynamic properties found in [25] is used in place of the table.

A flow restriction, placed between two control volumes, determines the flow rate of mass and energy between them. The flow rate depends on pressure and temperature of the adjacent control volumes. In many cases, the equations of the equivalent ideal flow for compressible gas is used for this purpose. The equation used for the model [24] assumes an isentropic process across the restriction. Therefore, any forms of energy gain or loss should be accounted for to satisfy the conservation laws.

In case of a compressor and a turbine, the model requires a performance data map from measurement or a manufacturer. The map represents the relationship between the pressure ratio across the device and rotating speed of the rotor, ω_{TC}; versus the corrected mass flow, $\dot{m}_{\mathrm{corr,TC}}$; and the isentropic efficiency of the process, η_{TC}. Having acquired the mass flow and the efficiency, the energy flow in and out can be calculated assuming an isentropic process. Then the torque for each turbomachine can be calculated as

$$\tau = \frac{\dot{m}\Delta h}{\omega_{\mathrm{TC}}} \tag{5}$$

where, $\dot{m}$ and Δh are actual mass flow and change in enthalpy across the machine. A dynamic equation is used for the mechanical rotation of the turbocharger.

$$J\dot{\omega} = \tau_{\mathrm{turb}} - \tau_{\mathrm{comp}}, \tag{6}$$

where τ_{turb} and τ_{comp} are the torque by the turbine and compressor, J is the rotational inertia of the turbocharger, and ω is the angular velocity of the turbocharger.

The whole engine block, including intake and exhaust valves, fuel injection system, cylinders, and pistons is simplified to a single flow restriction model. In this model, the input is the pressure, p_{AR}; and temperature of the air receiver, T_{AR}; the engine speed, ω_{eng}; and the fuel rack position, u. Mass flow through this restriction model can be determined given a known volumetric efficiency of the process, η_{vol}.

$$\begin{aligned}
\dot{m}_{\mathrm{in}} &= \eta_{\mathrm{vol}}\left(p_{\mathrm{AR}}\right)\rho_{\mathrm{AR}} V_d \frac{\omega_{\mathrm{eng}}}{n_s \pi}, \\
\dot{m}_{\mathrm{out}} &= \dot{m}_{\mathrm{in}} + \dot{m}_b, \\
\dot{m}_b &= m_{f,\max} u \frac{\omega_{\mathrm{eng}}}{n_s \pi},
\end{aligned} \tag{7}$$

where ρ_{AR} is the density of the gas in the air receiver, V_d is the displacement volume, n_s is the number of stroke of the engine cycle, $\dot{m}_b$ is the burned fuel mass flow, and $m_{f,\max}$ is the maximum amount of fuel injected per cycle. Energy flow in and out of the cylinder is calculated by

$$\begin{aligned}
\dot{E}_{\mathrm{in}} &= \dot{m}_{\mathrm{in}} h_{\mathrm{AR}}\left(p_{\mathrm{AR}}, T_{\mathrm{AR}}\right), \\
\dot{E}_{\mathrm{out}} &= \dot{E}_{\mathrm{in}} + \dot{m}_{b,\mathrm{out}}\mathrm{LHV}\left(1 - C_{HT} - \frac{1}{\mathrm{LHV}\cdot\mathrm{SFC}}\right),
\end{aligned} \tag{8}$$

where h_{AR} is the enthalpy of air from the air receiver volume, LHV is low heating value of the fuel, C_{HT} is the heat transfer ratio, and SFC is the specific fuel consumption. The torque output of the engine is

$$\tau_e = \frac{\dot{m}_{b,\mathrm{out}}}{\omega_{\mathrm{eng}}\cdot\mathrm{SFC}}. \tag{9}$$

The overall mean value engine system model is presented in Fig. 5. Both compressor and turbine model require ambient pressure and temperature as boundary conditions for the system. The input to the overall model is fuel rack position and engine speed; the output is pressure and temperature of the air receiver, volumetric efficiency, and torque. The first three outputs are used in order to calculate the mass trapped in the cylinder per cycle, which is further used to calculate the maximum allowable injected fuel amount according to given fuel-air equivalent limit. This functionality is termed as smoke limiter, which ensures that the charge in the cylinder is lean enough to avoid visible smoke during rapid power output increase.

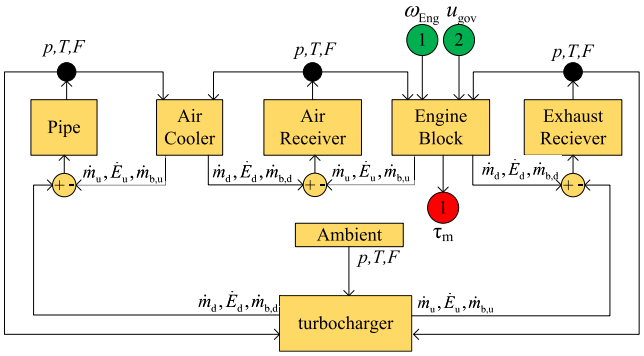

FIGURE 5. Mean value engine system model scheme, including a turbocharger, a charge air cooler and incylinder process.

A short-coming of such a model is that it requires extensive parameter identification in order to achieve reasonable accuracy. However, a well-defined engine model can be used for different cases if the main physical variables are converted into per unit values. This may cause inaccurate response characteristics since machines at various power range should have somewhat different time scales. The step load response characteristics of a genset can be used to calibrate the overall model including the governor to match the given characteristics. Such characteristics can be found in the manufacturer's documentation, e.g. [29].

2) RATE CONSTRAINED MODEL

A simplified model can be used for engines where the fuel rate is constrained such that the combustion is complete. In Section II-C, simulations show that this is the case for maritime engines due to the conservative rate constraints set by the engine manufacturers. A simplified model that ignores the air dynamics and requires only one parameter is

$$\tau_m = k_u u, \tag{10}$$

where τ_m is the torque output of the diesel engine, and k_u is the gain from fuel rate to mechanical torque. The fuel consumption is found by a Willans approximation [22].

3) SHAFT SPEED DYNAMICS

The engine shaft speed dynamics is given by

$$\dot{\theta} = \omega\omega_b, \tag{11}$$

$$\dot{\omega} = \frac{1}{2H}\left(-D_f\omega + \tau_m - \tau_e\right), \tag{12}$$

where θ is the mechanical angle, ω is the per unit mechanical angular velocity, ω_b is the base mechanical angular velocity, and the windage friction constant is denoted D_f. This is derived by the swing equation and assuming linear damping. H is defined as

$$H = \frac{1}{2}\frac{J\omega_b^2}{P_b}, \tag{13}$$

where J is the rotational inertia of the generator set and P_b is the base power of the generator set [20].

4) GOVERNOR

The two engine models use the same governor, which is based on droop control [30]. The commanded fuel index is then calculated by a PID controller with back calculation to avoid wind-up of the integrator term. The derivative of the frequency is calculated by using the *dirty derivative*.

$$\omega_{\text{ref}} = \omega_{\text{NL}} - K_{\text{droop}}p, \tag{14}$$

$$u = K_p(\omega_{\text{ref}} - \omega) + K_i\xi - K_d\hat{\omega}, \tag{15}$$

$$\dot{\xi} = \omega_{\text{ref}} - \omega + K_b(u_{\text{saturated}} - u), \tag{16}$$

$$\dot{\hat{\omega}} = N(\omega - \hat{\omega}), \tag{17}$$

where the K_d, K_i, K_p, and K_b are the derivative, integration, proportional, and back-calculation gain. The per unit produced generator power is denoted p. The symbols ω_{ref}, ω_{NL}, and $\hat{\omega}$ are the reference frequency, setpoint no-load frequency, and estimated time derivative of the frequency.

For the rate constrained model, an additional constraint on the fuel index is needed to avoid too large temperature variations in the cylinder and sooting due to too little air for complete combustion. This constraint is predefined and, therefore, static. In the case study, the engine is allowed to increase the fuel index with 20% of the rated output and then increase the fuel index with $8.1\%/s$. This is found by tuning the engine model response to fit recovery time and frequency drop in [29].

For the mean value model, a smoke limiter constrains the governor's command. The amount of air available for a cycle is

$$m_{\text{air}} = \eta_{\text{vol}}\frac{p_{\text{AR}}V_d}{RT_{\text{AR}}}, \tag{18}$$

where η_{vol} is the volumetric efficiency, p_{AR} and T_{AR} are the pressure and temperature at an air receiver, R is the specific gas constant and V_d is the displacement volume of a cylinder. Given the maximum fuel-air equivalent ratio, $F_{\max}$, the maximum fuel index, $u_{\max}$, is given by

$$u_{\max} = m_{\text{air}}\frac{F_{\max}f_s}{m_{\text{f,inj}}}, \tag{19}$$

where f_s is the stoichiometric fuel-air ratio and $m_{\text{f,inj}}$ is the amount of maximum fuel injection per cycle. In the case study, $F_{\max}$ is chosen as 1 in order to give a reasonable engine response.

F. ENERGY STORAGE DEVICES

ESDs include batteries, capacitors, fuel cells, or any other device capable of providing and consuming power on demand. They are accounted for by the PMS as available power reserve, and depending on the control strategy adopted by the PMS, it might substitute a fast load reduction strategy. The inner dynamics in the energy storage devices are disregarded, since it is assumed that its dynamics are much faster than the remaining components.

All components included here are simplified, since the losses are modeled using an efficiency table. This method makes it simple to include and model more components with data provided by the manufacturers.

G. THRUSTERS

The thrusters are modeled as propellers which are driven by electrical motors. The propellers are assumed to be fixed pitch, while the speed is variable. No thruster-thruster or thruster-hull interaction losses are included. It is assumed that the torque of the electrical motor is perfectly controlled. A frequency converter is often used to control the motor. The time scale of the dynamics of the frequency converter is much faster than the dynamics of the mechanical part of the thruster drives, and it is therefore neglected. A speed controller is used to control the thrust. The open water characteristics are used to calculate the desired shaft speed, from the requested thrust. The thrust is given by [31]

$$T_a = \text{sign}(n)K_T\rho D^4 n^2, \tag{20}$$

where K_T is the thrust coefficient found from open water tests, ρ is the density of water, D is the propeller diameter, and n is the shaft speed. This gives the desired shaft speed

$$n_d = \text{sign}(T_d)\sqrt{\frac{|T_d|}{K_T\rho D^4}}. \tag{21}$$

The desired thrust signal must be smoothed since the desired thrust is typically calculated at 1 Hz. Large power fluctuation will occur at each thruster command update instant if this is not done. A second order filter is therefore used for this task.

The four-quadrant model of the propeller presented in [32], is used to calculate the actual thrust and torque of the thruster. The benefit of this model is that it models *wind milling* (i.e., shaft speed and torque have different signs).

The advance velocity of the propeller is assumed to be equal to the relative velocity of the vessel. This means that wave-propeller interaction due to vessel motion is included, but wave-propeller interaction due to wave-induced particle motion is not included [33].

This model was first presented by [34]. The thrust and torque coefficients are defined as

$$C_T = \frac{T_a}{\frac{1}{2}\pi R^2 \rho V_{0.7}^2}, \tag{22}$$

$$C_Q = \frac{Q_a}{\frac{1}{2}\pi R^3 \rho V_{0.7}^2}, \tag{23}$$

where T_a is the thrust, R is the radius of the propeller, and Q_a is the propeller torque. $V_{0.7}$ is the undisturbed incident velocity to the propeller blade at radius $0.7R$ and is defined as

$$V_{0.7} = \sqrt{V_a + (0.7\omega R)^2}, \tag{24}$$

where ω is the angular velocity of the propeller shaft.

The angle of attack of the propeller at $0.7R$, β, is defined as

$$\beta = \arctan\left(\frac{V_a}{0.7\omega R}\right). \tag{25}$$

To estimate C_T and C_Q, a Fourier approximation as a function of β is used, with parameters from [32].

The power consumption of the thrusters are typically reduced after a fault by the fast load reduction. This is done by limiting the torque of the electrical motor driving the propeller. In practice, this is done by the frequency converter.

The thrust allocation needs an estimate of the power consumption of the thrusters. The four-quadrant model is not suitable for this purpose, as the advance velocity is not available for the thrust allocation. The power consumption by the electric thruster is therefore approximated by

$$p = k|f|^{1.5}, \tag{26}$$

where f is the thrust amplitude, and k is a constant which can be found from bollard pull test results or open water tests [31, Ch. 9]. Due to the approximation, the actual and approximated power consumption may be different.

H. OTHER COMPONENTS

The last model in the electrical power simulator is a block named *other loads*. It represents loads that do not directly influence the propulsion system and are modeled as time series of desired and actual power consumption. The load is divided into two parts: high and low priority loads. Both send a desired power consumption to the PMS. The PMS will then allocate power available back to these loads. The PMS will first allocate power to the high priority loads, which may be an emergency system. The thrusters will then get allocated the remaining power, before the low priority loads get the last remaining available power. The actual consumed power is set equal to the allocated power available.

I. VESSEL, ENVIRONMENT, OBSERVER, AND DP CONTROLLER

Models from the MCSim toolbox and MSS toolbox [8] are used to model the vessel. In the simulation cases we have chosen models suitable for DP operations. The MSS toolbox contains multiple vessel models, and the model should be chosen depending on the simulation case.

MCSim is a high fidelity vessel model for low speed simulations, which includes wave frequency motions and low frequency motions. The low frequency motions includes forces from slowly varying current, second order wave drift, mean wind, and wind gust, in addition to hydrodynamic and thruster forces from the vessel. Wave frequency motion is found by motion transfer functions. MCSim uses transfer functions which can be found from WAMIT [35].

The state observer is a passive observer based on [36], and the DP controller is implemented as a PID controller.

The fastest time scales of the vessel motion dynamics is the time scale of the wind gust, around 1 seconds. The slowest time scale is the change of the environmental condition, this is in the order of tens of minutes to hours or days. The environment is set constant, except for a slowly varying ocean current. Simulations are usually done using a shorter time horizon than the time scale of the change of environment condition. In such cases, the environment can be assumed to be constant during the simulation period.

II. VERIFICATION

Most of the models used in this simulator are well known models, which are already verified. However, the electric model, the rate constrained diesel engine model, and the parameters of the mean value diesel engine model need to be verified.

A. ELECTRIC MODEL

A generator model based on flux linkages is used to verify the electric model [20, Sec. 5.11]. Parameters for the model are found in [20, Table 5.10-1] and the simulations are done with two generators connected to the same load. The generator sets are operated with similar diesel engines, AVR, and governors for both models and generator sets.

For the steady-state model, the load is set to consume a constant power. The load of the flux-linkage model is set by a resistance, which gives the desired power consumption when the voltage is at the rated value.

In Fig. 6, the power, voltage, and frequency of the generators are plotted for a step increase of the load from 20% to 70%. Note that the simulated power of the steady-state model fits the power consumption of the flux-linkage model. A drop in the power of the flux-linkage occurs since the resistance of the load is suddenly increased, which also gives a voltage drop. The small difference afterward is mainly due to the different models of the load. The frequency is perfectly modeled, as expected since the power response is close for the two models. However, the voltage is not as well aligned

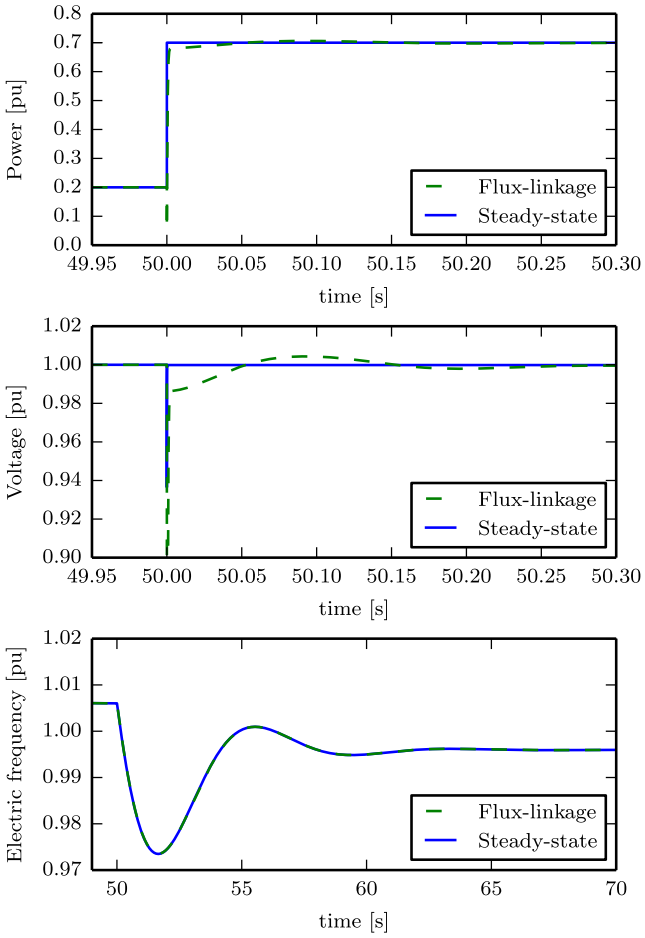

FIGURE 6. Simulation of a step increase of the load from 20% to 70% of the rated values. The simulations are done with the models described in Section I-D (steady-state) and models presented in [20, Sec. 5.11] (flux-linkage). Upper: power of generators. Middle: terminal voltage of generators. Lower: electric frequency of generators, note the difference in the time scale.

during the first tenth of a second. Both models are able to capture a drop in voltage. However, while the timescale of the drop is consistent between the model (few milliseconds), the magnitude is inconsistent (6.3% for steady-state model and 71% for the flux-linkage model). There are also some sub-transients which are not captured by the steady-state model.

In order to model the voltage accurately, a high fidelity model of the load is also needed. This may be difficult for a marine vessel consisting of many different consumers where each consumer needs to be modeled.

B. DIESEL ENGINE MODEL

A good diesel engine model should be able to predict fuel consumption as well as the engine dynamics in terms of speed under transient loads. It is crucial to get a correct fuel consumption curve because the model uses a prescribed cycle efficiency curve rather than actual cycle calculation in the cylinders. Such a curve can be obtained by fitting to the given fuel consumption data available for the engine.

However, the dynamic response of the engine arises from a combination of effects from multiple submodels of the system. The mean value model used in the simulator alone has about 50 parameters, of which some are arrays. Finding proper parameters and tuning the model can be a cumbersome process, even if the performance data of the engine is available. In order to ease the configuration process, one can use a well verified simulation model and normalize the output. However, the timescale of the engine dynamics may differ. Therefore, such a model should be re-tuned to match the dynamics of the engine of interest.

This can be done by tuning a limited number of parameters which have major influence on the engine response to the load changes. In this paper, the gains for the governor controller, the inertia of turbocharger, the inertia of generator set, and the maximum fuel-air ratio are chosen as tuning parameters. The response curve from the load acceptance test of a specific engine was used as reference. Then, simulation and optimization are used to curve-fit the simulated response with the reference data.

The mean value model used in this paper is a generic model for a medium speed four-stroke engine with a reasonable set of parameters. The reference engine is MAN 16V32/44CR which has power rating of 9.6 MW. The reference response curve for frequency recovery time and the frequency recovery time vs. step load amplitude plot are used to fit the engine response of the model to the measured value [29]. Frequency recovery time is defined as the time interval from the frequency deviates from the steady state band until it again enters the band according to ISO 8528-5. Such a band is assumed to be 1%, and the result of fitting is shown in the Fig. 7.

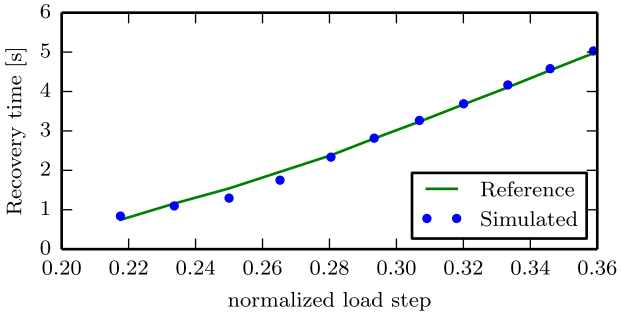

FIGURE 7. Dynamic response fitting of diesel engine.

C. RATE CONSTRAINED DIESEL ENGINE MODEL

As mentioned in Section I-E, diesel engine manufacturers constrain the rate of change of the throttle position. However, a smoke limiter will assure that the throttle position is limited such that complete combustion and maximum torque is achieved.

In Fig. 8, the earlier presented generator set is subjected to a load step from 20% active power to 60%. The figure shows the responses of the throttle position with and without the smoke limiter and the rate constraint of the

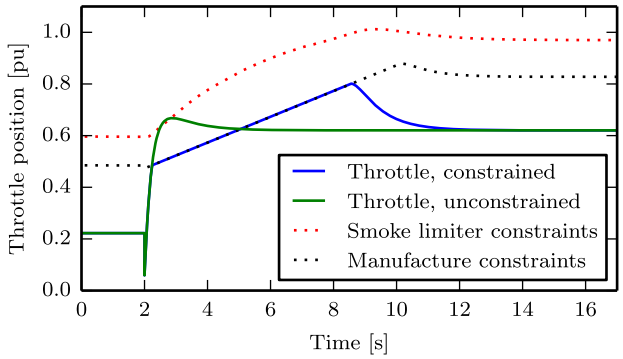

FIGURE 8. Throttle response of a load step, with and without constraints. The dotted lines represent the rate constraint of the manufacturer and the throttle constraint of the smoke limiter.

manufacturer activated. The constraints are also included, showing the smoke limiter level and the rate constraint. It is clear that the rate constraint from the manufacture are always lower than the smoke limiter. The smoke limiter can therefore be neglected. It should be noted that this result is only valid for this engine.

III. CASE STUDY

Three cases are analyzed, where the objective is to illustrate simulations that are only possible through a multi-domain simulator. It is noteworthy that the focus is in the qualitative analysis, but not on quantitative analysis, since the overall simulator is not quantitatively verified.

A drilling rig is used to illustrate the simulator capabilities, not only for fault scenarios but normal operations as well. The electrical system is shown in Fig. 3. The rig has three switchboards, which are connected in a ring configuration. Two generator sets are connected to each switchboard. The rated outputs of the diesel engines are 9.1 MW. In addition, two thrusters are connected to each switchboard with a rated output of 4.2 MW and a rated thrust of 506 kN. The thrusters' position are shown in Table 1. The rig pontoon length is 84.6 m, with total mass of 27×10^6 kg. The dynamic model is assuming low speed, as well as current is considered as a component of the vessel total speed, instead of a force. More details about the vessel can be found in [7].

TABLE 1. Thruster position on the drilling rig hull.

Thruster	Thruster type	X Position [m]	Y position [m]
1	Azimuth	-35	-27
2	Azimuth	-35	27
3	Azimuth	0	-27
4	Azimuth	0	27
5	Azimuth	35	-27
6	Azimuth	35	27

Besides the drilling rig, a hybrid supply vessel was modeled to verify the influence of energy storage devices on the vessel electrical stability. The electrical system is shown in Fig. 9, where a battery pack, a 2.2 MW generator, and a 3.3 MW generator are connected to each power bus. The thruster characteristics are described in Table 2. The vessel length is 80 m, with total mass of 6.2×10^6 kg.

TABLE 2. Thruster position and size on the supply vessel.

Thruster	Type	X Position [m]	Y position [m]	Max Power [MW]
1	Azimuth	-30	-5	2.7
2	Azimuth	-30	5	2.7
3	Tunnel	24	0	1.5
4	Tunnel	27	0	0.85
5	Tunnel	30	0	1.5

TABLE 3. Environmental condition summary for the simulation cases.

Simulation case	H_s [m]	T_p [s]	V_w [m/s]	V_c [m/s]
III-A	5	8.5	14	1
III-B	5	7	14	.3
III-C	4	7.7	12	1

A summary of the simulated environmental conditions is shown in Table 3. Wind, wave, and current direction in all simulation cases are always from north to south, the JONSWAP wave spectrum [37] and the NORSOK wind spectrum are used [31].

A. DP OPERATION SCENARIO

The first case study shows a typical DP operation. The goal is to demonstrate the load fluctuation due to the DP system's reaction to environmental forces and the power generated by the power producers. The position and heading setpoints are fixed at the origin. The buses are connected in a ring configuration, with all bus-tie breakers closed.

Fig. 10 shows the vessel surge position and electric bus frequency for the simulated case. Notice that the simulator is able to capture different time scales and time constants in the vessel positioning and the generator power. A power variation of same time scale as the wave frequency is clearly visible. In addition, the change of thruster setpoint gives ripples at 1 Hz.

B. BUS OPENING SCENARIO

During a DP operation, it is possible that one bus is isolated from the remaining grid due to a pre-fault detection, reverse power flow, etc. In this case, the interaction between the electrical system and the DP system is exemplified. Even though the maximum generated capability and thruster forces are unaltered, there is an instantaneous power surge in the buses due to the reconfiguration.

In the simulation, the vessel is in DP operation and heading north, with closed bus-tie and five generator sets running (two connected to each of the first two switchboards and one to the third switchboard). Switchboard 3 is separated from the other two switchboards, by opening the breakers connected to Switchboard 3 at $t = 200$ s. The power consumption is constrained by the fast load reduction, due to the increased load.

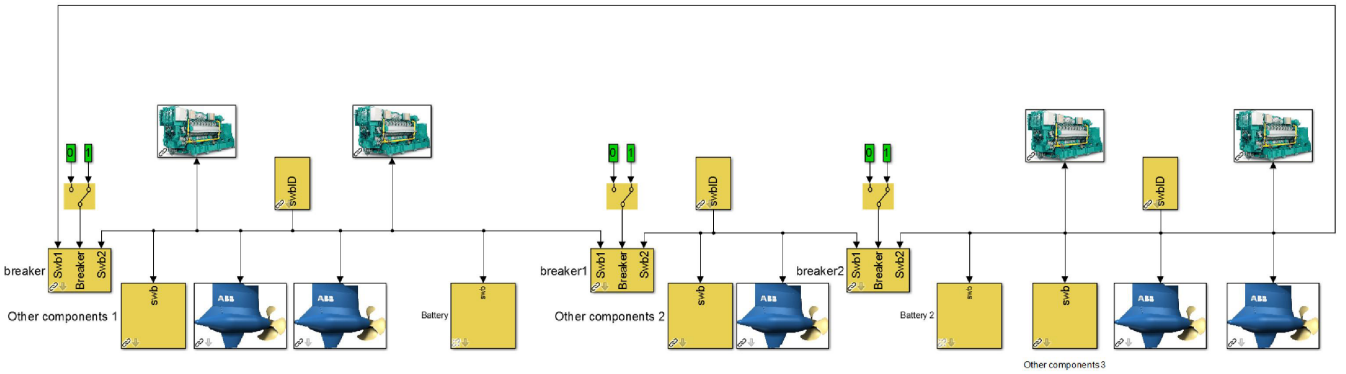

FIGURE 9. Power plant view of hybrid supply vessel used in simulations.

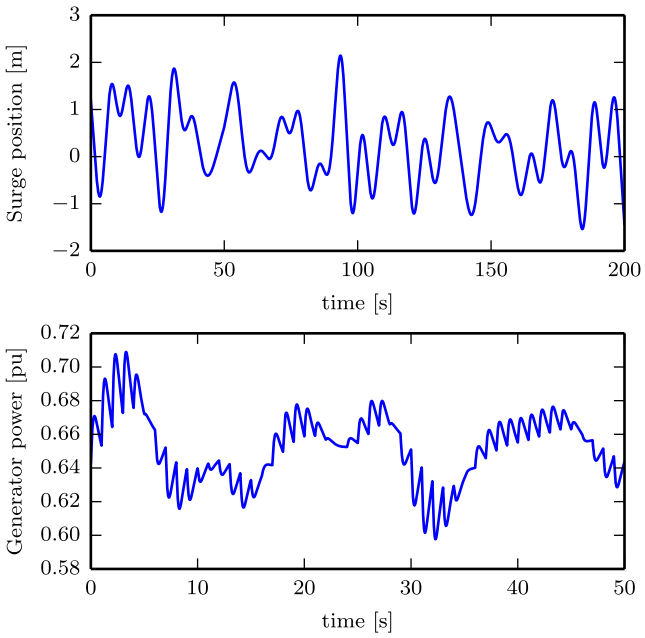

FIGURE 10. Results from simulation of drilling with DP, presented in Section III-A. Upper: surge position of the vessel. Lower: power produced by generators connected to the main bus in per unit.

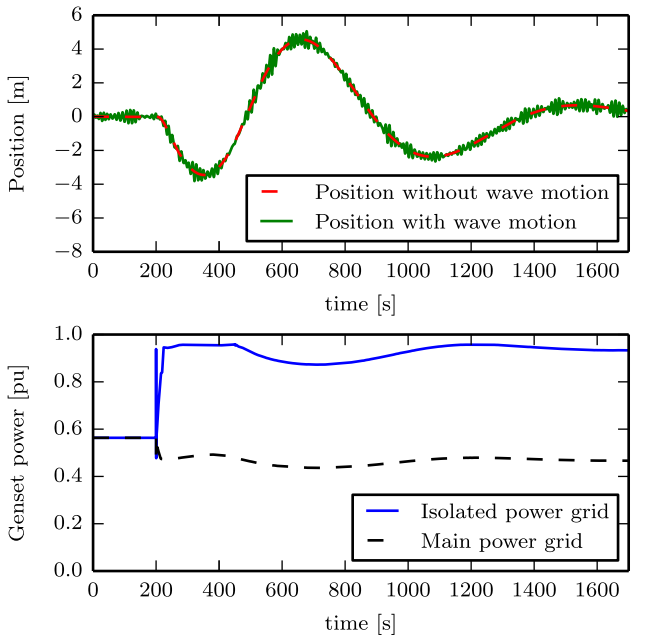

FIGURE 11. Results of the simulation case presented in Section III-B. The drilling vessel is in DP operation with closed bus-tie breakers. After 200 seconds the bus-tie breakers connected to Switchboard 3 is opened. Upper: Position deviation from the setpoint. The green solid line is the position deviation, while the red dashed line is the position deviation without the wave motion. Lower: power consumption for each bus. The blue solid line is the generator power at the isolated power grid (Swb. 3). The black dashed line is the generator power at main power grid (Swb. 1 and 2).

Fig. 11 shows the power bus reconfiguration effect on the dynamical positioning system. It is noticeable that when the power plant is reconfigured, the DP system positioning is influenced due to load reduction. This scenario can only be simulated with an integrated simulator, since the interdependency in the positioning system and electrical system is the factor leading to the positioning transient.

Both the vessel positioning and the filtered position (estimated by the state estimator) are presented in Fig. 11, since the wave frequency motion makes it harder to observe the mentioned effect.

C. ENERGY STORAGE DEVICES

The last case demonstrates how the addition of an energy storage device will increase overall safety, mostly due to the fact that the extra power injection in the bus will limit the frequency drop by the generator. The system presented here uses the supply vessel presented in Section III. All four generators and five thrusters are initially connected. An ESD is connected to the power system. After 1 second, one of the generators is abruptly disconnected from the power grid, generating a power surge for the remaining three generators. The ESD is controlled in frequency droop mode, but it will be connected only when the frequency drops below 98.5%.

The results from this scenario are shown in Fig. 12. The vessel position is virtually the same for both simulation cases, the main difference is that the frequency drop is much smaller in the case with ESD. It is known, that protection systems like load reduction and shedding will be activated when the

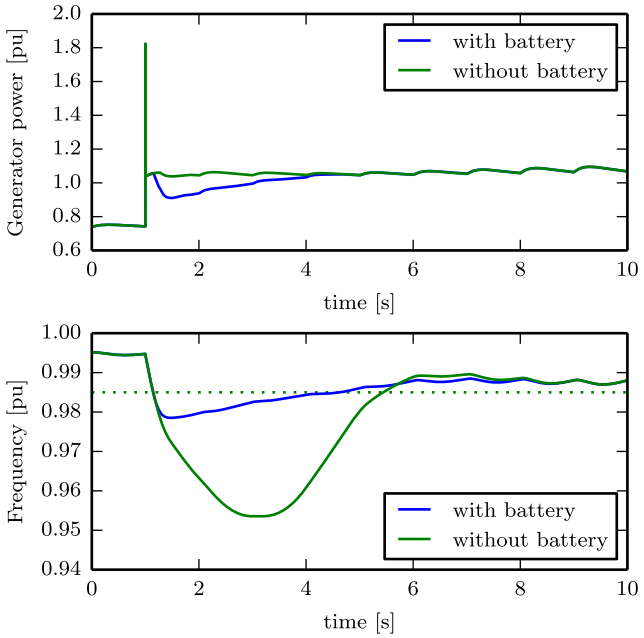

FIGURE 12. Results from presented in Section III-C. After 1 second one out of four generator is disconnected. Upper: generator power, with and without battery. Lower: electric frequency of the main bus, with and without battery.

frequency drops below 2% to 3%, possibly deactivating large power consumers, such as thrusters, drilling system, etc. If the frequency drops even further, it could lead to partial or even total blackout.

From the maintenance point of view, with smoother generator load variation, the wear and tear will be reduced, improving the generator working conditions and reducing maintenance costs.

This simulation shows that the simulator allows investigating the vessel and ESD dynamical behavior during a fault, in which the frequency drop is the main concern. The ESD is able to bound the frequency drop to a safe margin, potentially preventing a larger scale fault.

Other operation strategies may be implemented for the ESD, such as peak shaving, on-off operations, etc., if the simulator is properly set up.

CONCLUSION

In this article, a simulator for marine vessels electric propulsion is presented. The main contribution is the presentation and verification of the needed models for the integration of power plant simulation and vessel motion simulation. In addition to demonstrations of the integrated simulator, enabling qualitative analysis of cases that cannot be described with several decoupled simulators. Detailed models of the vessel, propeller, thruster drives, generator sets, and controllers are included in the system simulator, in addition to interaction effects between the components. A module based platform is presented, where models of different fidelity can be chosen. Due to the modularity, the simulator can be reconfigured to different vessels with electric propulsion, and different operations can be simulated. Simulink was used to implement the simulator. The case studies presented in the article show some capabilities of the simulator. More detailed simulations of, for instance, fault scenarios contribute to increased knowledge about the behavior of the electrical system, control systems, and safety functions. This may lead to more reliable vessels and safer operations in the future.

REFERENCES

[1] Marine Cybernetics. *Technology: Cybersea, N.D., Viewed 2014-12-12*. [Online]. Available: https://www.dnvgl.com/services/software-for-marine-operations-sesam-marine-2321, accessed Nov. 3, 2015.

[2] T. A. Johansen and A. J. Sørensen, "Experiences with HIL simulator testing of power management systems," in *Proc. Marine Technol. Soc. Dyn. Position Conf.*, 2009.

[3] L. Pivano, O. N. Smogeli, S. Muddusetti, and J. Ramsey, "Better analysis-better data-better decisions-better operational risk management=delivery of incident free operations: Enabled by DynCap," in *Proc. Marine Technol. Soc. Dyn. Position Conf.*, 2014.

[4] W. Ren, M. Steurer, and S. Woodruff, "Progress and challenges in real time hardware-in-the loop simulations of integrated ship power systems," in *Proc. IEEE Power Eng. Soc. General Meeting*, vol. 1. Jun. 2005, pp. 534–537.

[5] M. Steurer *et al.*, "Investigating the impact of pulsed power charging demands on shipboard power quality," in *Proc. IEEE Electr. Ship Technol. Symp. (ESTS)*, May 2007, pp. 315–321.

[6] Y. Xie, J. Sun, C. Miz, and J. S. Freudenberg, "Analysis and modeling of a DC hybrid power system testbed for power management strategy development," in *Proc. IEEE Vehicle Power Propuls. Conf. (VPPC)*, Sep. 2009, pp. 926–933.

[7] MSS. (2010). *Marine Systems Simulator*. [Online]. Available: http://marinecontrol.org

[8] T. Perez, Ø. N. Smogeli, T. I. Fossen, and A. J. Sørensen, "An overview of the marine systems simulator (MSS): A Simulink toolbox for marine control systems," *Model., Identificat. Control*, vol. 27, no. 4, pp. 259–275, Oct. 2006.

[9] T. I. Fossen, *Marine Control Systems: Guidance, Navigation and Control of Ships, Rigs and Underwater Vehicles*. Trondheim, Norway: Marine Cybernetics, 2002.

[10] A. J. Sørensen, E. Pedersen, and Ø. N. Smogeli, "Simulation-based design and testing of dynamically positioned marine vessels," in *Proc. Int. Conf. Marine Simulation Ship Maneuverability (MARSIM)*, Tokyo, Japan, 2003.

[11] T. Perez and M. Blanke, "DCMV a MATLAB/Simulink toolbox for dynamics and control of marine vehicles," in *Proc. 6th IFAC MCMC*, Girona, Spain, 2003.

[12] DNV-GL. *Software for Marine Operations—Sesam Marine*. [Online]. Available: http://dnv.com/services/software/products/sesam/sesam_marine, accessed Nov. 3, 2015.

[13] D. Bosich, M. Filippo, D. Giulivo, G. Sulligoi, and A. Tessarolo, "Thruster motor start-up transient in an all-electric cruise-liner: Numerical simulation and experimental assessment," in *Proc. Elect. Syst. Aircraft, Railway Ship Propuls. (ESARS)*, Oct. 2012, pp. 1–5.

[14] J. F. Hansen, A. K. Ådnanes, and T. I. Fossen, "Mathematical modelling of diesel-electric propulsion systems for marine vessels," *Math. Comput. Model. Dyn. Syst., Methods, Tools Appl. Eng. Rel. Sci.*, vol. 7, no. 3, pp. 323–355, 2001.

[15] D. Radan, "Integrated control of marine electrical power systems," Ph.D. dissertation, Dept. Marine Technol., Faculty Eng. Sci. Technol., Norwegian Univ. Sci. Technol., Trondheim, Norway, Apr. 2008.

[16] T. A. Pedersen and E. Pedersen, "Bond graph modelling of marine power systems," *Math. Comput. Model. Dyn. Syst., Methods, Tools Appl. Eng. Rel. Sci.*, vol. 18, no. 2, pp. 153–173, 2012.

[17] T. I. Bø and T. A. Johansen, "Scenario-based fault-tolerant model predictive control for diesel-electric marine power plant," in *Proc. MTS/IEEE OCEAN*, Bergen, Norway, Jun. 2013, pp. 1–5.

[18] T. Bø, T. A. Johansen, and E. Mathiesen, "Unit commitment of generator sets during dynamic positioning operation based on consequence simulation," in *Proc. 9th IFAC Conf. Control Appl. Marine Syst.*, 2013, pp. 1–5.

[19] T. I. Bø *et al.*, "Real-time marine vessel and power plant simulation," in *Proc. ASME 34th Int. Conf. Ocean, Offshore Eng. (OMAE)*, May/Jun. 2015.

[20] P. C. Krause, O. Wasynczuk, and S. D. Sudhoff, *Analysis of Electric Machinery and Drive Systems*, 3rd ed. New York, NY, USA: McGraw-Hill, Feb. 2013.
[21] J. Benajes, J. M. Luján, V. Bermúdez, and J. R. Serrano, "Modelling of turbocharged diesel engines in transient operation. Part 1: Insight into the relevant physical phenomena," *Proc. Inst. Mech. Eng. D, J. Automobile Eng.*, vol. 216, no. 5, pp. 431–441, 2002.
[22] L. Guzzella and C. H. Onder, *Introduction to Modeling and Control of Internal Combustion Engine Systems*, 2nd ed. Berlin, Germany: Springer-Verlag, 2010.
[23] A. Chow and M. L. Wyszynski, "Thermodynamic modelling of complete engine systems—A review," *Proc. Inst. Mech. Eng. D, J. Automobile Eng.*, vol. 213, no. 4, pp. 403–415, Apr. 1999.
[24] J. Heywood, *Internal Combustion Engine Fundamentals*. New York, NY, USA: McGraw-Hill, 1988.
[25] F. Zacharias, "Analytical representation of the thermodynamic properties of combustion gases," SAE Tech. Paper 670930, 1967.
[26] K. K. Yum and E. Pedersen, "Transient performance and emission prediction of diesel engine system using pseudo bond graph model," in *Proc. 9th Asia-Pacific Conf. Combustion*, Gyeongju, Korea, 2013.
[27] E. Pedersen and H. Engja, "A bond graph model library for modelling diesel engine transient performance," in *Proc. ISME*, vol. 2. Tokyo, Japan, 2000, pp. 447–455.
[28] M. W. Chase, *NIST-JANAF Thermochemical Tables*. Washington, DC, USA: American Chemical Society, 1998, p. 9.
[29] *32/44CR Project Guide—Marine*, MAN Diesel & Turbo, Augsburg, Germany, 2013, p. 56. [Online]. Available: http://marine.man.eu/four-stroke/project-guides
[30] Woodward. (2004). *Governing Fundamentals and Power Management, Viewed 2014-12-15*. [Online]. Available: http://woodward.com/workarea/downloadasset.aspx?id=2147483987
[31] A. J. Sørensen, "Marine control systems: Propulsion and motion control systems of ships and ocean structures," 2nd ed., Dept. Marine Technol., Norwegian Univ. Sci. Technol., Trondheim, Norway, Tech. Rep. Report UK-13-76, 2013.
[32] Ø. N. Smogeli, "Control of marine propellers," Ph.D. dissertation, Dept. Marine Technol., Faculty Eng. Sci. Technol., Norwegian Univ. Sci. Technol., Trondheim, Norway, 2006.
[33] A. J. Sørensen and Ø. N. Smogeli, "Torque and power control of electrically driven marine propellers," *Control Eng. Pract.*, vol. 17, no. 9, pp. 1053–1064, Sep. 2009.
[34] I. Y. Miniovich, "Investigation of hydrodynamic characteristics of screw propellers under conditions of reversing and calculation methods for backing of ships," Bureau Ships (BuShips), Washington, DC, USA, Tech. Rep. AD0700702, 1960.
[35] C.-H. Lee. (Oct. 1995). WAMIT theory manual. Massachusettes Institute of Technology. [Online]. Available: http://www.wamit.com/Publications/tmanual.pdf
[36] T. I. Fossen and J. P. Strand, "Passive nonlinear observer design for ships using Lyapunov methods: Full-scale experiments with a supply vessel," *Automatica*, vol. 35, no. 1, pp. 3–16, Jan. 1999.
[37] K. Hasselmann *et al.*, "Measurements of wind-wave growth and swell decay during the joint north sea wave project (JONSWAP)," Deutsches Hydrographisches Inst., Hamburg, Germany, Tech. Rep. 8-12, 1973.

TORSTEIN I. BØ was born in 1988. He received the M.Sc. degree in marine technology from the Norwegian University of Science and Technology, Trondheim, Norway, in 2012, where he is currently pursuing the Ph.D. degree with the Department of Engineering Cybernetics. His research interest include control systems and environmentally-friendly marine power systems.

ANDREAS R. DAHL received the M.Sc. (siv.ing.) degree in engineering cybernetics from the Norwegian University of Science and Technology (NTNU), in 2013, where he is currently pursuing the Ph.D. degree. He joined the Department of Marine Technology, NTNU, in 2013. His research interests include shipboard electrical power systems, dynamic positioning, fault tolerance, and nonlinear and multiagent control.

TOR A. JOHANSEN received the M.Sc. and Ph.D. degrees. He worked at SINTEF Electronics and Cybernetics, as a Researcher. He was appointed as an Associated Professor with the Norwegian University of Science and Technology (NTNU), Trondheim, in 1997, and was promoted to Professor in 2001. In 2002, he co-founded the company Marine Cybernetics AS, where he was the Vice President until 2008. He is currently a Principal Researcher with the Center of Excellence on Autonomous Marine Operations and Systems and the Director of the UAV Laboratory at NTNU. He has authored over 100 articles in international journals and numerous conference articles and book chapters in the areas of control, estimation, and optimization with applications in the marine, automotive, biomedical, and process industries.

EIRIK MATHIESEN received the B.Sc. degree from Vestfold University College in 1996. He joined Kongsberg Maritime in 1997, as a Project Engineer, and has been involved in the power management design for drillships and semisubmersible vessels on more than 50 installations. He joined Royal Norwegian Navy, in 1996, as an Electrical Supervisor. He is currently a Principal Engineer with Kongsberg Maritime, responsible for the application development of power management and dynamic positioning integration. He is a Co-Holder of patents on dynamic load prediction, dynamic load compensation, and dynamic power plant protection.

MICHEL R. MIYAZAKI was born in São Bernardo do Campo, Brazil, in 2010. He received the B.S. degree in mechanical engineering from the University of São Paulo, São Paulo, Brazil, and the M.S. degree in mechanical engineering from the University of São Paulo, in 2013. He is currently pursuing the Ph.D. degree with the Marine Technology Department, Norwegian University of Science and Technology, Trondheim, Norway.

His research topics involves variable speed engines, dc grids, energy storage devices, and fuel consumption minimization.

EILIF PEDERSEN received the M.Sc. degree in marine engineering from the Norwegian Institute of Technology, Norway, in 1983. He has been with the Norwegian Marine Technology Research Institute, as a Senior Research Engineer. He joined The Norwegian University of Science and Technology, in 2001, as an Associate Professor. His areas of expertise are in the field of modeling methodology and simulation of dynamic multidisciplinary and mechatronic systems focusing on machinery system dynamics, internal combustion engines, vibrations, thermal- and hydraulic machines, fuel-cell system dynamics, and hybrid power plants for marine applications.

ROGER SKJETNE (M'99) received the M.Sc. degree in control engineering from the University of California at Santa Barbara, Santa Barbara, CA, USA, in 2000, and the Ph.D. degree from the Norwegian University of Science and Technology (NTNU), Trondheim, Norway, in 2005, for which the thesis was awarded the Exxon Mobil Prize for best Ph.D. thesis in applied research.

He was an Electrician with Aker Elektro AS, working on numerous oil installations for the North Sea. From 2004 to 2009, he was with Marine Cybernetics AS, working on the hardware-in-the-loop simulation for testing safety-critical marine control systems. Since 2009, he has been a Professor of Marine Control Engineering with the Department of Marine Technology, NTNU, where he is currently the Leader of the Research Group on Marine Structures. His research interests are within Arctic stationkeeping operations and ice management systems for ships and rigs, environmentally robust control of shipboard electric power systems, and nonlinear control theory for motion control of single and groups of marine vessels.

Prof. Skjetne serves as the Project Manager of the KMB Arctic DP Research Project, the Leader of the ice management work package with the Center for Research-Based Innovation Sustainable Arctic Marine and Coastal Technology, and an Associated Researcher with the Centre of Excellence Centre for Ships and Ocean Structures and Autonomous Marine Operations and Systems.

ASGEIR J. SØRENSEN (M'89) received the M.Sc. degree in marine technology and Ph.D. degree in engineering cybernetics from the Norwegian University of Science and Technology (NTNU), in 1988 and 1993, respectively. From 1989 to 1992, he was a Research Scientist with the Norwegian Marine Technology Research Institute. In 1993, he was a Research Scientist with ABB Corporate Research Norway. In 1994, he became the R&D Coordinator/Project Manager with ABB Industri. In 1996, he was appointed to Manager of Positioning Systems with ABB Industri. From 1998 to 2001, he was the Technical Manager with Business Area Automation Marine and Turbochargers, ABB Automation. In 2002, he and his five partners founded the company, Marine Cybernetics AS, where he was acting as the President and Chief Executive Officer until 2010. DNV GL acquired Marine Cybernetics in 2014. In 2012 and 2015, he became a Co-Founder of the NTNU spin-off companies Ecotone AS and SwimM AS, respectively. Since 1999, he has held the position of Professor of Marine Control Systems with the Department of Marine Technology, NTNU. He is currently the Director of the Centre for Autonomous Marine Operations and Systems with the Department of Marine Technology and Department of Engineering Cybernetics, NTNU. He has authored over 180 scientific articles and book chapters on ride control of SES, dynamic positioning of ships and semi-submersibles, guidance and control of underwater vehicles, control of marine structures, modeling and control of propulsion systems, power and energy management systems, and HIL testing and verification of control systems. He has graduated more than 90 M.Sc. and 16 Ph.D. Candidates. He has also together with colleges established the Marine Cybernetics Laboratory and the Applied Underwater Robotics Laboratory at NTNU.

LAXMINARAYAN THORAT (M'15) was born in India in 1987. He received the B.Tech. degree in instrumentation engineering from the University of Nanded, India, in 2009, and the M.Tech. degree in systems and control engineering from IIT Bombay, Mumbai, India, in 2011.

He is currently pursuing the Ph.D. degree with the Norwegian University of Science and Technology, Trondheim, Norway. He joined General Motors Technical Center India, Bangalore, in India, in 2012, as a Design Engineer. Since 2013, he has been with the Department of Marine Technology, Norwegian University of Science and Technology.

His main areas of research interest are shipboard electrical power system, generators, and their control systems.

KEVIN K. YUM received the B.Sc. degree in naval architecture and ocean engineering from Seoul National University, Korea, in 2001, and the M.Sc. degree in marine engineering from the Norwegian University of Science and Technology, in 2012.

He is currently pursuing the Ph.D. degree in marine engineering. He served as an Accounting Officer in the Army of Korea for 28 months from 2001, and was a Sales Engineer with Samsung Heavy Industries for seven years from 2003. His main fields of interest are numerical simulation of internal combustion engine system, physical system modeling and technical development, and commercial evaluation of LNG cargo handling system and marine system in the ship and offshore unit.

He was awarded second place in the Young Scientist Award in the EuroKorean Conference on Science and Technology, in 2015.